Nanoscale

ROYAL SOCIETY OF CHEMISTRY

PAPER

View Article Online
View Journal | View Issue

Cite this: *Nanoscale*, 2020, **12**, 3249

Temperature, strain and charge mediated multiple and dynamical phase changes of selenium and tellurium†

Salih Demirci,[a,b] Hikmet Hakan Gürel,[c] Seymur Jahangirov *[a] and Salim Ciraci *[d]

Received 17th July 2019,
Accepted 23rd December 2019

DOI: 10.1039/c9nr06069c

rsc.li/nanoscale

Semiconducting selenium and tellurium in their 3D bulk trigonal structures consist of parallel and weakly interacting helical chains of atoms and display a number of peculiarities. We predict that thermal excitations, 2D compressive strain and excess charge of positive and negative polarity mediate metal–insulator transitions by transforming these semiconductors into different metallic crystal structures. When heated to high temperature, or compressed, or charged positively, they change into a simple cubic structure with metallic bands, which is very rare among elemental crystals. When charged negatively, they transform first into body-centered tetragonal and subsequently into the body-centered orthorhombic structures with increasing negative charging. These two new structures stabilized by excess electrons also have overlapping metallic bands and quasi 2D and 1D substructures of lower dimensionality. Since the external charging of crystals can be achieved through their surfaces, the effects of charging on 2D structures of selenium and tellurium are also investigated. Similar structural transformations have been mediated also in 2D nanosheets and free-standing monolayers of these elements. These phase changes assisted by phonons are dynamical, reversible and tunable; the resulting metal–insulator transitions can occur within very short time intervals and may offer important device applications.

1. Introduction

Two group-VI elements, selenium and tellurium, in their bulk trigonal structures (specified as t-Se and t-Te), as well as in their various compounds exhibit unusual features. Pressure and shear can induce structural transitions with complex electronic structures, which comprise new quantum states of matter:[1] Much earlier, phase transitions in Se and Te were traced by single-crystal X-ray diffraction using a high-pressure diamond anvil cell.[2] In fact, six different phases of 3D Se were revealed by high-pressure X-ray diffraction experiments.[3] Theoretical studies based on Density Functional Theory (DFT) predicted similar 3D phases of Te under pressures of 0–200 GPa.[4] Despite the absence of inversion symmetry, t-Te is predicted to become a strong topological insulator or a topological metal under the application of shear or uniform and uniaxial strain, respectively.[5] Both t-Se and t-Te possess multiple Weyl nodes. The Weyl semimetal phase[6] with broken inversion symmetry is predicted to occur under pressure.[7] Binary and ternary alloys of Se and Te are found to be topological insulators. 2D monolayers of specific transition metal dichalcogenides, especially $MoTe_2$, have been deduced as phase-change materials, PCM.[8–13] Neutral ultrathin Te films are predicted to have four (α-, β-, γ- and δ-) phases.[14] It has been demonstrated that some of these less stable phases could be stabilized by sole-charge doping, which could also induce phase transition among them.[15] All these studies give clues to possible facile structural phase transitions of t-Se and t-Te crystals driven by specific excitations.

In their global equilibrium structure, t-Se and t-Te are composed of 1D vertical, helical chains (or coils) of atoms situated at the corners of a hexagonal lattice displaying a quasi 1D character as shown in Fig. 1a. This conjecture is justified by the fact that in t-Se (t-Te), despite the strong intrachain covalent bonding and the resulting cohesive energy of 2.88 (2.71) eV per atom, the attractive interaction between chains is

[a]*UNAM-Institute of Materials Science and Nanotechnology, Bilkent University, Ankara 06800, Turkey. E-mail: seymur@unam.bilkent.edu.tr*
[b]*Department of Physics, Kırıkkale University, Kırıkkale 71450, Turkey*
[c]*Department of Information Systems Engineering, Kocaeli University, 41380 Kocaeli, Turkey*
[d]*Department of Physics, Bilkent University, Ankara 06800, Turkey. E-mail: ciraci@fen.bilkent.edu.tr*

† Electronic supplementary information (ESI) available: The phonon and energy bands of t-Se and t-Te structures; energy bands of new sc, bct, bco structures; calculated values for structural parameters and energetics in Table S1; band gap closing under electrostatic charging; *ab initio* MD calculations of new phases. See DOI: 10.1039/c9nr06069c

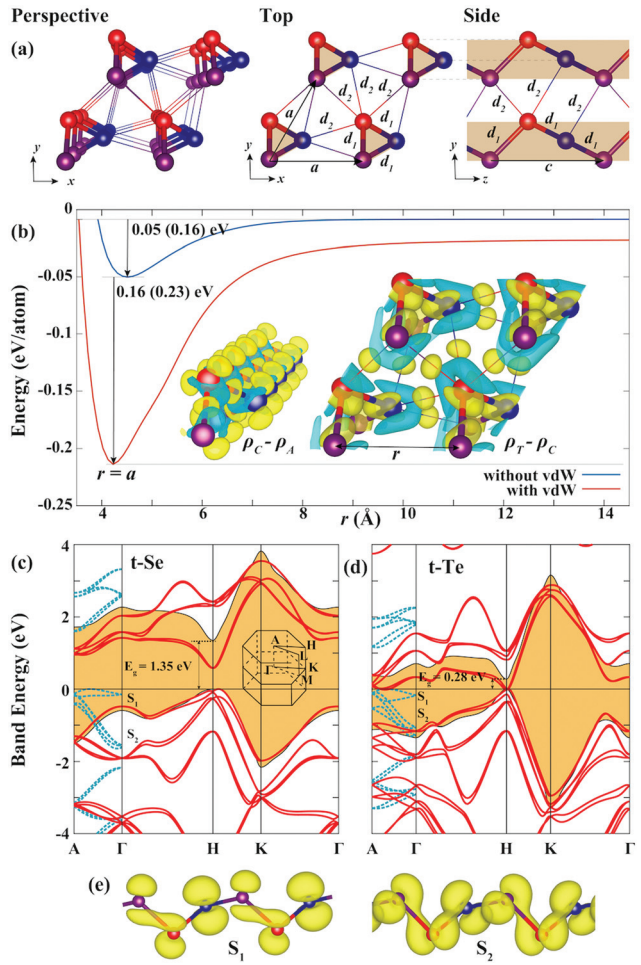

Fig. 1 (a) Perspective, side and top views of the optimized atomic structure of (3D) bulk t-Se and t-Te (T = 0 K, strain ε = 0, excess charge q = 0). Lattice constant a, intrachain d_1, and interchain d_2, distances are indicated. Helical chains (or coils) are situated at the corners of hexagons. (b) Variation of the energy (per atom) with interchain distance r calculated with and without vdW interaction. Helical chains of Se (Te) are held by an energy of 0.21 (0.39) eV per atom; 0.05 (0.16) eV per atom of it is the chemical interaction. The isosurfaces of the difference of the total charge density of t-Se and the charge density of its isolated coil, $\rho_T-\rho_C$, as well as the difference between ρ_C and the charge density of free Se atoms, $\rho_C-\rho_A$ are also shown. Regions of charge accumulation and depletion are indicated by yellow and turquoise colour, respectively. Small charge accumulation in yellow at the centre of d_2 shows the weak bond charge between chains. Electronic energy band structure of t-Se (c), and t-Te (d) calculated by PBE + SOC along selected symmetry directions. The fundamental band gaps, which are opened after HSE + SOC calculations, are shaded. The bands of isolated, free helical chains with flat S_1, and dispersive S_2 bands are also shown by dashed lines along the chain axis, Γ–A. (e) The charge density isosurfaces of S_1 and S_2 states.

rather weak and is composed of chemical interaction of 0.05 (0.16) eV per atom and van der Waals (vdW) interaction of 0.16 (0.23) eV per atom as shown in Fig. 1b. Fig. 1b also indicates how the energy varies with the interchain distance, d_2 relative to the optimized intrachain bond length, d_1. This situation is reminiscent of the weak interlayer, but strong intralayer interaction in vdW solids[16,17] like graphite and layered h-BN. The charge density analysis provides further insight into the bonding. The charge of free helical chains tends to move from the inner to outer side to constitute lone-pairs. However, when condensed in the trigonal phase, charge is dispersed in the interchain region forming small bond charge between every nearest two atoms of adjacent 1D chains associated with weak covalent bonds as shown by the inset in Fig. 1b. This explains how the isotropy in specific properties arises despite the quasi 1D structure.

Surprisingly, the electrical conductivity measured along and across the chains is quite isotropic.[18] This peculiarity was attributed to the delocalization of lone-pairs.[19] The energy band structures of t-Se and t-Te calculated using the Perdew–Burke–Ernzerhof functional (PBE)[20] including spin–orbit coupling (SOC) and corrected by the hybrid functional (HSE)[21] are presented in Fig. 1c and d (see Methods of calculations). Both crystals are semiconductors with a HSE fundamental band gap of E_g = 1.35 eV and 0.28 eV, respectively. In particular, t-Te displays large spin–orbit splitting, unusual band dispersions and a small band gap, which are crucial for topologically non-trivial behavior. The comparable, but significant dispersions of the bands along the chain axis (Γ–A direction) and perpendicular to the chains (Γ–K direction) support the isotropy in electrical conductivity.[18] Additionally, S_1 and S_2 bands of an isolated chain in Fig. 1c and d together with their charge distributions in Fig. 1e indicate that bulk t-phases are electronically rather different from isolated 1D chains (full phonon and energy bands are presented in the ESI†).

In this paper, further to the above peculiar features we unveil another unusual, but fundamentally and technologically critical behavior of Se and Te crystals. Based on first-principles calculations we predict that either thermal excitation or 2D uniform compressive strain, or electrostatic charging can induce multiple and dynamical phase changes in bulk t-Se and t-Te. These phase transformations occur spontaneously and are followed by metal–insulator transitions. Namely, t-Se and t-Te being semiconducting crystals under ambient conditions, they can transform into rare, 3D crystals in the metallic state. Notably, when electrostatically charged, not only 3D trigonal crystals, but also their 2D nanosheets and free-standing monolayers, *i.e.* α-tellurene, can transform into different metallic structures. These metal–insulator transitions, which can take place reversibly, can find critical applications in opto-electronic devices and electric field induced composite materials.

2. Methods of calculations

First-principles calculations based on DFT were carried out using two different basis sets, plane waves and local orbitals which are applied by VASP[22–25] and SIESTA[26] packages, respectively. In plane-wave calculations, we used projector-augmented wave (PAW) potentials[27] and the exchange–correlation potential within the generalized gradient approximation (GGA) with

the Perdew, Burke, and Ernzerhof (PBE) functional.[20] Wave functions are expanded in plane-wave basis sets up to the electron kinetic energy cut-off of 275 eV for Se and 228 eV for Te crystals. Brillouin zone (BZ) integration is performed with an automatically generated 12 × 12 × 10 *k*-point grid in the Monkhorst–Pack scheme.[28] Ionic relaxation is realized by the conjugate gradient algorithm, which optimizes the structure. All atoms in the supercell are fully relaxed until the energy difference between the successive steps is less than 10^{-5} eV and the force on each atom is less than 10^{-2} eV Å^{-1}. In addition, maximum pressure on the lattice has been lowered down to 0.1 kBar. We also apply the Heyd–Scuseria–Ernzerhorf (HSE) hybrid functional method[21] to obtain corrected band gap values. The HSE06 functional is constructed by mixing 25% of the Fock exchange with 75% of the PBE exchange and 100% of the PBE correlation. We chose specific van der Waals (vdW) corrections based on the comparison of structure parameters of t-Se and t-Te optimized using different vdW methods with the experimental structure parameters. We then chose the Tkatchenko–Scheffler method with iterative Hirshfeld partitioning (PBE-TS/HI).[29,30] Since the plane-wave method under periodic boundary conditions may fail in first-principles calculations of charged systems comprising large spacing between surfaces or atomic rods,[31] we performed also calculations using the local basis set, where the eigenstates of the Kohn–Sham Hamiltonian are expressed as a linear combination of numerical atomic orbitals. A 2720 eV cut-off energy for Se and 2312 eV for Te crystals are used and the self-consistent field calculations are performed with a mixing rate of 0.1. The grid of 11 × 11 × 9 is used for *k*-points in BZ. Core electrons are replaced by norm-conserving, nonlocal Trouiller–Martins pseudo potentials.[32] For the exchange–correlation potential, we employ a nonlocal functional that includes van der Waals interactions (VDW-DF) named as (DRSLL).[33,34] All of our conclusions concerning the effect of the charging are obtained from atomic orbital calculations using SIESTA.[26] The dynamical stability analyses of neutral phases are performed by calculating the phonon spectrum using a small displacement method. The force constant (dynamical) matrix is constructed by slight displacement of atoms in a 6 × 6 × 6 supercell using the results of first-principles plane-wave calculations. PHON software has been used to determine the necessary displacements and to calculate the phonon dispersions using the obtained force constants.[35] Those structures having vibration modes with frequencies $\omega^2 > 0$ for all *k*-points in the first BZ are considered to be stable at $T = 0$ K. The thermal stability of both neutral and charged systems is tested by *ab initio* molecular dynamics (MD) calculations at finite temperature. The time step between ionic iterations was taken to be 2 fs. Velocities are rescaled at the end of every 50 steps to match the desired temperature. In the MD simulation shown in Fig. 2a, the system is heated from 100 K to 1000 K within 2 ps; its atomic configuration is constructed by taking the average of the atomic position in the last 500 ionic steps.

The cohesive energy E_c(P) per atom of a phase (P) made of either Se or Te atoms is calculated from the expression, E_c(P) = $[nE_T(\text{Se/Te}) - E_T(\text{P})]/n$, in terms of the optimized total energies of free constituent atoms, Se or Te, E_T(Se/Te), and the optimized total energy of the given phase E_T(P), n being the number of atoms in the unit cell. These optimized total energies of different systems are calculated with similar calculation parameters and unit cells. The positive value of the cohesive energy indicates binding of constituent free atoms. The formation energy E_f of a P phase relative to the structure of global minimum is obtained by subtracting the cohesive energy of the parent crystal t-Se or t-Te from E_c(P), namely E_f(P) = E_c(P) − E_c(t-Se/t-Te). Negative formation energy implies that the phase P either corresponds to a local minimum in the Born–Oppenheimer surface, or it is unstable. As it will be explained in forthcoming sections, the stability of new phases here is maintained either by excess charge, or compressive 2D strain, or thermal energy. Calculated values of structural parameters, E_c, E_f and band gaps E_g are presented in Table 1. Here the differences between the values calculated using different basis sets are attributed to different pseudo potentials and other

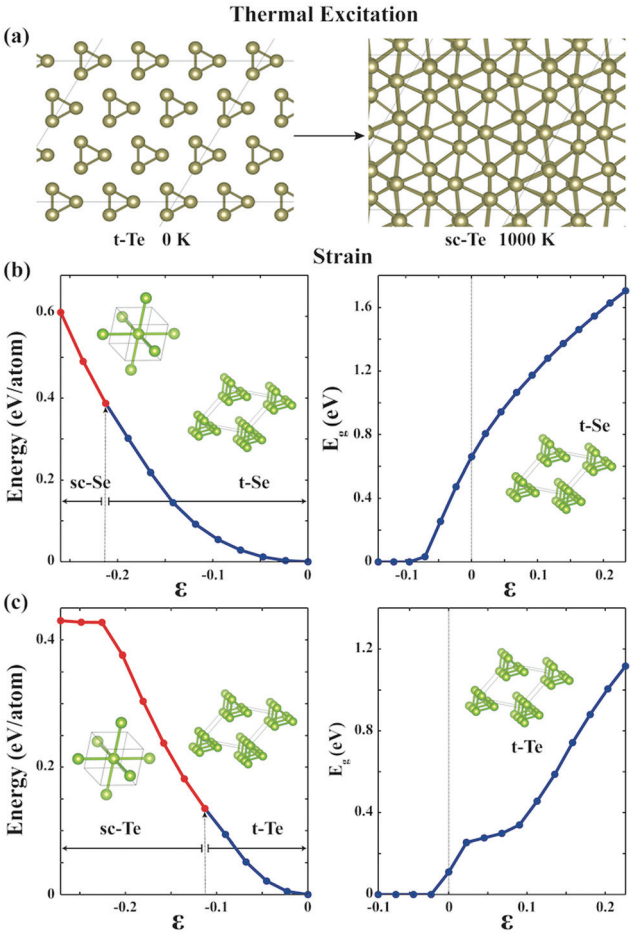

Fig. 2 (a) Snapshots of atomic configurations taken from the *ab initio* MD calculations of t-Te at $T = 0$ K transforming to sc-Te at $T = 1000$ K. (b) Right: structural transformation of t-Se under 2D uniform strain, ε to sc-Se. Left: the curve shows the variation of PBE fundamental band gap E_g with ε. (c) Same as (b) for t-Te.

Table 1 Se and Te elements; structures and lattice types, lattice parameters *a*, *b* and *c*; shortest bond d_1; secondary bond d_2; bond angle θ; cohesive energy per atom E_c; formation energy at T = 0 per atom relative to the global minimum, E_f; the fundamental band gap calculated by PBE + SOC, $E_{g,PBE+SOC}$; those calculated by HSE + SOC, $E_{g,HSE+SOC}$. Values are calculated by using the plane wave basis set[22–25] at the neutral state, but those given in parenthesis are calculated by using the local basis set[26] in the neutral state of t-phases, as well as the charged state of new phases. References are for the previous theoretical and experimental values

Element	Structure	Lattice	a, Å	b, Å	c, Å	d_1, Å	d_2, Å	θ, degree	E_c, eV per atom	E_f, eV per atom	$E_{g,PBE+SOC}$, eV	$E_{g,HSE+SOC}$, eV
Se	t	Hexagonal	4.23 (4.51)	4.23 (4.51)	5.11 (5.12)	2.43 (2.45)	3.34 (3.55)	103.81 (103.44)	2.88 (3.27)		0.58 (1.08)	1.35, 1.74,[7] 2.00[36]
	sc	Simple cubic	2.82 (2.85)	2.82 (2.85)	2.82 (2.85)	2.82 (2.85)		90 (90)	2.74 (3.01)	−0.14 (−0.26)	Metal (metal)	
	bct	Body centered tetragonal	2.63 (2.80)	2.63 (2.80)	7.71 (7.80)	2.63 (2.80)	3.85 (3.90)	90 (90)	2.68 (3.02)	−0.20 (−0.25)	Metal (metal)	
	bco	Body centered orthorhombic	(2.80)	(3.99)	(7.08)	(2.80)	(3.54)	(90)	(3.10)	(−0.17)	(metal)	
Te	t	Hexagonal	4.43 (4.82)	4.43 (4.82)	5.93 (5.91)	2.90 (2.87)	3.42 (3.74)	101.24 (101.86)	2.71 (3.05)		Semimetal (0.58)	0.28, 0.31,[7] 0.32[37]
	sc	Simple cubic	3.18 (3.20)	3.18 (3.20)	3.18 (3.20)	3.18 (3.20)		90 (90)	2.69 (3.00)	−0.02 (−0.05)	Metal (metal)	
	bct	Body centered tetragonal	3.00 (3.20)	3.00 (3.20)	7.85 (8.77)	3.00 (3.20)	3.92 (4.38)	90 (90)	2.55 (2.95)	−0.16 (−0.10)	Metal (metal)	
	bco	Body centered orthorhombic	(3.16)	(4.46)	(8.00)	(3.16)	(4.00)	(90)	(3.04)	(−0.01)	(metal)	

approximations. However, our conclusions are drawn from the values of optimized structural parameters, energies and structures calculated by the same method. Therefore, our conclusions are consistent; they are not affected by the values of lattice constants predicted by different methods within 5–6% difference. The cohesive energies calculated using plane waves for q = 0, and the local basis set for q = 0, as well as for $q \neq 0$, are consistent, since the cohesive energies of new phases are always smaller than the parent t-phases corresponding to global minima. The band gaps of t-Se and t-Te calculated with the plane wave basis set and subsequently corrected with HSE + SOC appear to agree with the measured band gaps.

3. Temperature, strain and charge induced phase changes

The first indication of phase transitions has been obtained by thermal excitations of the 3D trigonal structures in the global minimum. *Ab initio* MD simulations at high temperature performed with a variable unit cell size in Fig. 2a demonstrate that the t-Te structure transforms to a simple cubic structure, sc-Te, by squeezing d_2, when heated as high as $T \sim 1000$ K. In fact, this phase transition would occur already for T much smaller than 1000 K, if the simulation time could be taken much longer. Higher temperatures are needed for the transition from t-Se to sc-Se due to the higher energy difference, ΔE between them.

It is well known that the sc-structure is very rare among elemental crystals; Po (polonium, extremely radioactive group-VI element just below Te in the Periodic Table) was known to be the only element that has a simple cubic primitive cell in its ground state, and is stabilized through the relativistic mass-velocity and Darwin terms.[38] It was argued[38] that neutral t-Te cannot change into the sc-structure even when mass-velocity and Darwin terms are included.

The causes of facile phase transitions under diverse types of excitations can be sought in the trigonal structure. Since the sc-structure can be viewed as a trigonal structure having a rhombohedral unit cell with the angle θ = 90° between diagonals, it wouldn't be difficult for the t-phase to transform back into the cubic structure by thermal or other excitations. Conversely, t-structures can be derived by deforming the simple cubic lattice,[39] so that each Se or Te atom has two nearest, covalently bonded neighbors in the chain at a distance d_1 and four second nearest neighbors between the chains at a distance d_2 as depicted in Fig. 1a.

The 2D uniform compressive strain gives rise to a similar effect on the structure of the 3D t-Se and t-Te as shown in Fig. 2b and c. When a 3D t-phase is compressed in the *xy*-plane by decreasing the distance, a between helical chains, the lattice constant, c expands. However, for specific values of 2D uniform strain, $\varepsilon_x = \varepsilon_y = (a - a_0)/a_0$, the atomic structure can change to the sc-structure, which is accompanied by a metal–insulator transition. This transition occurred for t-Se (t-Te) at ε_x = 0.21(0.09) with an increase of the total optimized energy

ΔE = 0.39(0.14) eV per atom and a decrease of volume $\Delta V = (V - V_0)/V_0$ = 0.28(0.12). Notably, the predicted threshold strain necessary for the phase change to the sc-structure appears to be too high for t-Se due to relatively higher energy. Here, the strain energy necessary for the phase change from t- to sc-structure in Fig. 2c, ΔE = 0.14 eV per atom, appears to be consistent with the energy of the thermally induced phase change to the same structure discussed above. Previous X-ray diffraction experiments[2,3] and a recent study[4] predicting new phases (allotropes) of t-Te under high hydrostatic pressure are in compliance with the present findings. As for the 2D tensile strain, it does not induce any structural transition in t-Se and t-Te, since the binding interaction between helical chains is rather weak.

The electric field and hence induced electrostatic charging are electronically the most interesting excitation, which can exfoliate single layers from multilayers,[40,41] control the adatom adsorption and desorption,[42,43] store energy[44–46] and tune the electronic structure[47–49] in 2D materials. Charging can be achieved by external electric field or by optical excitation, whereby valence electrons occupy conduction states by creating e–h pairs maintaining the charge neutrality. Here, we considered direct and external charging by depletion or injection of electrons and examine its effect on the atomic structure.

In analogy with the exfoliation of 2D monolayers, like graphene and BN, from their parent layered structures under excess positive charge,[40,41] one normally contemplates whether the helical chains are disassembled from t-Se and t-Te by electrostatic charging. With this premise, structurally anisotropic t-Se and t-Te are optimized by minimizing the total energy, atomic forces and lattice constants under electron deficiency ($q > 0$) and excess electrons ($q < 0$) within DFT. Owing to the difficulties to be encountered using a plane wave basis set,[31] optimization of charged structures has been carried out using the local basis sets.[26] In contrast to the expectations, the charged trigonal crystals were not disassembled into free chains for both polarities. Apparently, as a result of charging, the crystal potential is modified, whereby band gaps are closed, some vibration modes lack restoring force and thus their corresponding frequencies attained imaginary values leading to instability. Eventually, the original structures underwent a series of structural phase transformation: we found that when charged positively, t-Se and t-Te change into sc-structures as occurred under thermal excitation or 2D uniform compressive strain. As the positive excess charge is increasing, the parent t-phases first start to shrink, subsequently once the excess charges exceed well-defined threshold values ($q_{th} > 0.42$ e per atom in t-Se or $q_{th} > 0.25$ e per atom in t-Te) they are transformed into the sc-structure, one of its body diagonals coinciding with the axis of the chain of the parent t-phases. On the other hand, when charged negatively, the interchain distances of t-Se and t-Te first increase, then they transform first into the body-centered tetragonal (bct) and subsequently into the body-centered orthorhombic (bco) structure with increasing excess electronic charge.

It should be noted that all these new structures are metallic due to closed band gaps. Additionally, once the excess charge exceeded well-defined threshold values, they occurred spontaneously in the course of structure optimization from the t-phases of the global minima. Even if the angles might deviate from 90° during structure optimizations, structures with right angles mark the lowest energy. Moreover, these structural transformations are followed by volume changes, ΔV for example, −15% for sc- (which is well compared with that obtained under compressive ε), +10% for bct- and +36% for bco-Te. To eliminate possible constraints, which may be imposed by using a single cell in structure optimizations, the variation of energy with excess charge was also investigated in the 2 × 2 × 2 supercell, which resulted in the same phase changes.

The excess charge is attained by depopulating valence band states for positive polarity or by populating the empty conduction band states for negative polarity, which are performed self-consistently. Coulomb divergences in the charged systems were hindered by adding an equal amount of background charge of the opposite polarity in the SIESTA code and then the structure optimizations are carried out by minimizing the total energy.[26] It should be noted that the electrostatic charging of bulk Se and Te is quite different from their doping by foreign atoms. The latter results in dramatic local changes in the crystal potential. The total energies in these new phases attained within 3D periodic boundary conditions with background charge may not be uniquely defined.[50] To eliminate the effect of the background charge, the calculated energy *versus* charge variation was detrended by subtracting its linear part revealed in an earlier study.[10] Linear variation of the total energy with excess charge was also shown by the theory dealing with the quantum electronic stress and quantum Hook's law for Al and Si crystals.[51] The resulting variations of energies of Se and Te with excess charge in Fig. 3a and b show a series of structural transformations driven by charging. This is a surprising and important result.

As the excess electronic charge of t-Se in Fig. 3a exceeds the threshold charge, q_{th} = −1.17 e per atom, it transforms to a new, bco-phase, which attains its minimum energy for q_0 = −1.25 e per atom. Between the t-Se and bco-Se, there is, however, another phase called body-centered tetragonal, bct-Se, which cannot form directly from the t-phase through a phase transition, since its energy curve, $E_{bct}(q)$ lies higher, and does not intersect the energy curve of the t-phase, $E_t(q)$. Nonetheless, this phase may continue to exist in the range of excess charge $0 > q > -0.83$ e per atom once it was formed in the bct-structure at high temperature. Incidentally, bct-Se can be constructed by stacking Se monolayers with a 2D square lattice according to the *AA′AA′*... stacking sequence (where each Se atom of one monolayer *A* being located above the centers of a square of adjacent monolayers *A′*) with the interlayer distance much larger than the Se–Se bond. The body centered orthorhombic (bco) structure of Se can also be viewed as if it is constructed by stacking of Se monolayers with a 2D rectangular lattice. Alternatively, the same bco-structure can also be con-

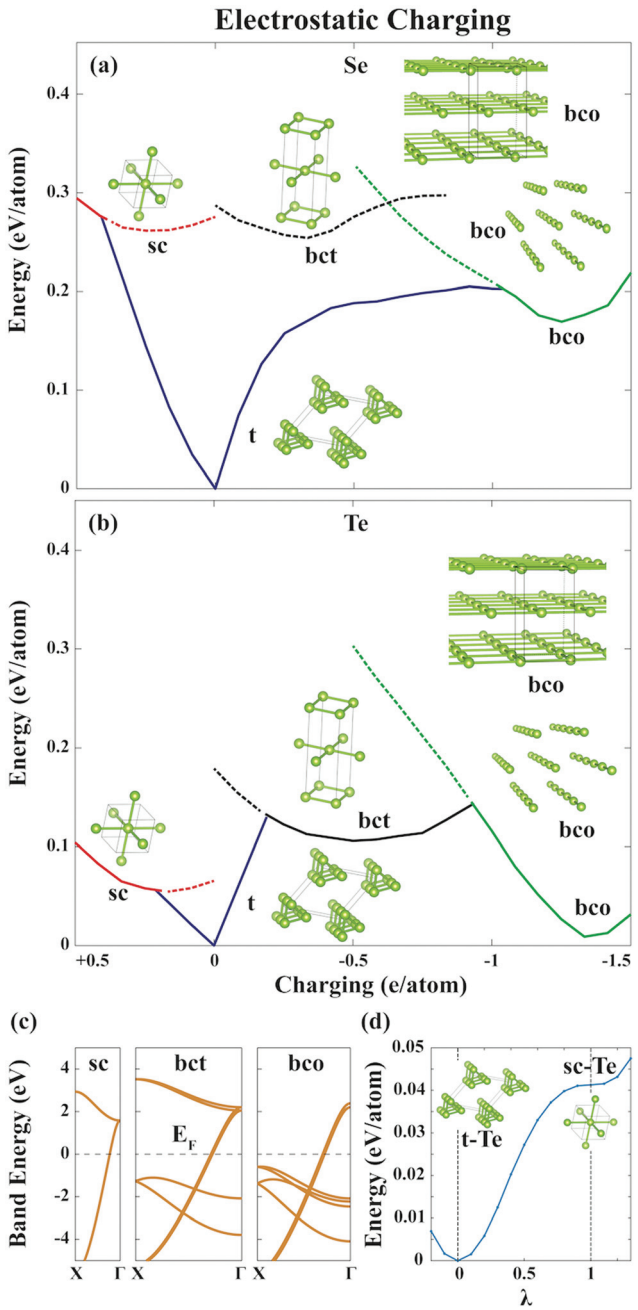

Fig. 3 Phase changes of semiconducting t-Se and t-Te mediated by electrostatic charging. All energies are calculated using a local basis set[26] and corrected to eliminate the effect of the background charge. (a) Variation of the optimized energy (per atom) of t-Se with excess charge q (in units of $\pm e$ per atom), which undergoes three different structural transformations (phases) with different lattice types, *i.e.* simple cubic (sc); body centred tetragonal (bct); body centred orthorhombic (bco). 2D square monolayers in the bct lattice, 2D rectangular monolayers and 1D linear chains in bco are indicated as substructures. (b) Similar for t-Te. (c) The metallic bands of these new sc-, bct- and bco-phases are shown along the X–Γ direction. Zero of energy is set at the Fermi level. (d) Energetics of smooth transition between t-Te and sc-Te with λ defining intermediate structural parameters as explained in the text.

structed from Se monatomic linear chains placed at the corners of a body centered hexagon as if it is the bundle of quasi 1D structures. In Fig. 3b, t-Te undergoes similar phase transformation when charged negatively, but at different charge values. Since the energy curve of t-Te intercepts the energy curves of both sc-phase for $q > 0$ and bct-phases for $q < 0$, the phase transitions take place spontaneously at well-defined values of q. Also, the transition from the bct-phase to bco-phase is spontaneous for the same reason. Similar to Se, these phases of Te can be viewed as if they are constructed from 2D or 1D substructures.

At this point we note that stable monolayers of free-standing Se and Te (named selenene and tellurene) have been predicted recently based on first-principles calculations. These are buckled square selenene and rectangular tellurene,[52] as well as α-Te (tellurene in the 1T-MoS_2 structure), metastable β-Te and γ-Te structures.[14] It was also predicted that the metastable (α, β, γ and δ) phases found in ultrathin Te films can be stabilized by the charge doping.[15] The substructures, namely 1D linear chains, 2D planar square and rectangular monolayers deduced above can be stabilized only by electrostatic charging, when they are free standing. In Fig. 3c the metallic bands of sc-, bct-, and bco-structures are shown along the X–Γ direction of BZ. Full energy bands of these new structures as well as the bands of their free-standing (1D and 2D) substructures presented in the ESI† corroborate that the substructures are, in fact, weakly interacting low dimensional structures.

4. Spontaneity and reversibility

Here we emphasize that the energy *versus* excess charge curves $E(q)$ presented in Fig. 3a and b are obtained by starting from t-structures in equilibrium and by optimizing it for different values of excess charge q. While a particular phase remains stable for a well-defined range of excess charge, it changes spontaneously to a different one when q exceeded a well-defined threshold value, where the $E(q)$ curve of the previous phase and that of the new one intersect. For sc-Se (sc-Te) $q_{th} > q_0$ and $E_{sc}(q_{th})-E_{sc}(q_0) \cong 0.02(0.01)$ eV per atom. The energy involved in this phase transition mediated by the positive excess charge, $\Delta E = E_{sc}(qth) - E_t(q = 0) \cong 0.28(0.05)$ eV per atom is small. Similar relations are valid for bct and bco phases with $q < 0$.

Whether a phase that occurred for a well-defined excess charge q can continue to exist when $q \to 0$ (similarly, for $T \to 0$ K or for $\varepsilon \to 0$ in temperature and strain driven phase changes, respectively) is crucial for the operation of Se and Te crystals as a switch. This issue concerns the energy ranges of the new phases marked by dashed lines in Fig. 3a and b and is closely related to the bistability of two phases for the same value of q. To clarify it, the energetics of structural transition from t-Te to sc-Te is investigated for the neutral case, namely $q = 0$. To this end, structural parameters of t-Te can be altered to form a three-atom supercell of sc-Te. Hence, we introduce the parameter that defines intermediate structural parameters as

it runs between $0 \leq \lambda \leq 1$ interpolating the structural parameters of t-Te to sc-Te, respectively. As seen in Fig. 3d, the t-phase smoothly changes to the sc-phase with increasing energy. Conversely, as the energy is lowered, sc-Te can directly transform to the energetically favorable t-Te without any energy barrier. This situation is consistent with the total energy *versus* q curve in Fig. 3b, as well as with the phase changes from the low-energy, global t-phase to high-energy sc-phase under 2D uniform compressive strain or thermal excitation; all these phase changes are followed by an increase of energy, ΔE. This situation is different from the transition from one phase to the other neutral one (both corresponding to different minima in the Born–Oppenheimer surface) overcoming an energy barrier. Also, the specific phonon modes of sc-Te, as well as other phases, which were stabilized under excess charge, attained imaginary frequencies, $\omega^2 < 0$, if they are calculated for $q = 0$. This indicates a dynamical instability at $T = 0$ K, since the sc-phase is not a local minimum for $q = 0$. As a result, these phases were prone to an instability at $q = 0$, whereupon their bistability at $q = 0$ is ruled out, but their *reversibility* is confirmed.

Next, the stability of these sc-, bct- and bco-phases driven by excess charge in Fig. 3a and b against the thermal excitations is ensured by performing *ab initio* molecular dynamics (MD) calculations at 400 K for 6 ps for q_0 corresponding to their minimum energy configurations (their snapshots are shown in the ESI†). It is found that these sc-, bct- and bco-phases of Se and Te maintain their stability above room temperature. Recently, it has been reported that the similar stabilization of some metastable allotropes of borophene by excess charge can be realized.[53,54]

5. Phase changes in 2D nanosheets (slabs) and monolayers

The crucial question one has to address is how the charging can be accomplished realistically within the 3D periodic boundary condition to attain the predicted phase changes. This is analogous to the question of how the energy bands of bulk solids calculated within 3D periodic boundary conditions are compared to the real situations. As realistic energy bands including the effects of surfaces can be calculated for slabs within the supercell geometry, here slabs having two surfaces within the supercell geometry constitute the proper model to allow external charging like gating of a device. Also, the excess charges can accumulate at the surfaces by populating or depopulating energy bands localized at the surfaces of metallized slabs (or nanosheets). This model is also in compliance with recent experiments.[40,55] To this end, we considered neutral and ideal monolayer (1L), 3L and 5L slabs of t-Te, as examples. Interestingly, when neutral, 1L consisting of three atomic planes of t-Te atoms was reconstructed spontaneously and formed the monolayer of α-tellurene having the 1T-MoS_2 structure. Similarly, the 3L slab was also reconstructed and formed a layered α-tellurene with *AAA* stacking in agreement with that reported recently by Zhu *et al.*[14] As for the 5L slab, it was not reconstructed, but relaxed with minute changes of interlayer spacing for $q = 0$. However, under the excess charge, the surface layers of the 5L slab became charged and concomitantly they underwent a phase change. When charged by $q = 0.33$ e per atom corresponding to a surface charge of approximately 100 μC cm^{-2}, the t-phase of the 5L slab changed to the sc-phase as shown in Fig. 4a. Similarly, when charged negatively, the structure of both surfaces changed to the bct like structure with the t-phase at the center and complex transition structures at the interface between the surfaces and center as depicted in Fig. 4b. Notably, the effect of charging can be better deduced from thicker slabs, which requires really high computational power. Further to these slab calculations, we also investigated the response of the α-tellurene monolayer to electrostatic charging. While this monolayer keeps its T-structure under $0 \leq q \leq 1$ e per atom, it changes to a new phase stabilized by an excess charge of $q \cong -0.4$ e per atom in the course of structure optimization. Atomic configurations of the semiconducting, neutral α-tellurene in T-phase and this

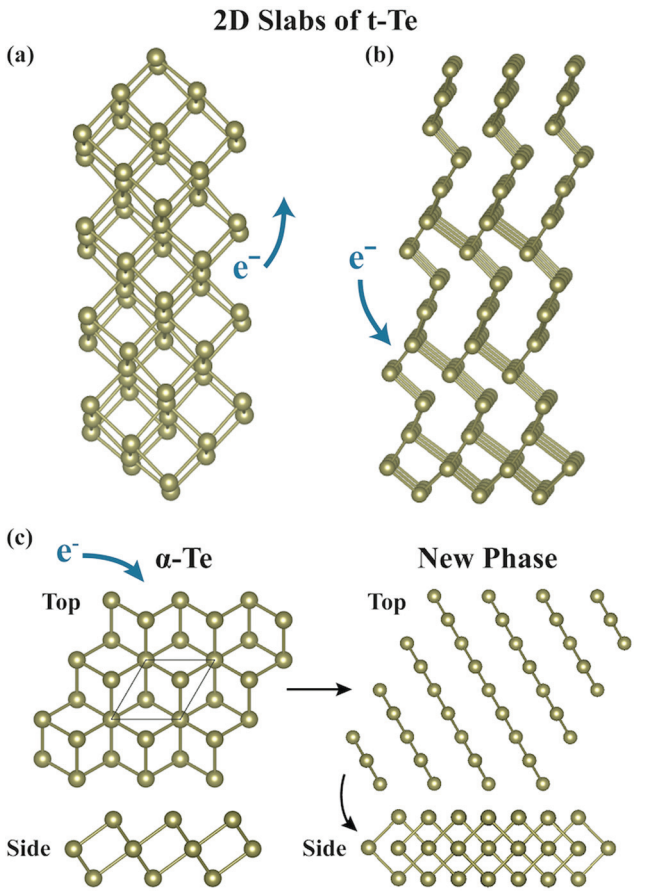

Fig. 4 Phase changes of the 5 L t-Te slab under electrostatic charging. (a) 5 L t-Te slab changes into the sc-structure under positive charging, $q > 0$. (b) The slab changes into the bct-structure under negative charging, $q < 0$. (c) Atomic configurations of the semiconducting T phase of the α-tellurene monolayer and its new phase occurring for $q < -0.4$ e per atom.

new quasi 1D phase consisting of widely spaced very narrow stripes (or atomic chains constructed from squares) are presented in Fig. 4c.

6. Discussion and conclusions

Reversible metal–insulator transitions have been realized by changing the phase of specific materials, called phase change materials, PCM with various excitations, such as thermal, optical (laser), strain, electrostatic, adatom (molecule adsorption) *etc*. For example, very thin (2D) semiconductor 1H-$MoTe_2$ can change from the semiconducting H-phase to metallic T′-phase in a very short time interval by injecting excess charge or by gating.[8–13] These electrically driven and reversible phase transitions with 2–3 ns response time give rise to dramatic changes in conductivity. Therefore, they are of extreme importance to various electronic, optical and fast switching devices, as well as to non-volatile memory applications, since their sudden switch is not limited by the transit times of carriers.[56]

In the past, the structural transitions of covalently bonded crystals of group-V and group-VI elements, in particular, those of PCM materials were attributed to Peierls (symmetry breaking) instability.[57] The resonant bonding concept is also utilized to explain fast and dynamical change from one phase to other *via* soft phonon modes.[57] All the phases predicted in this study have energies slightly higher than those of their parent structures and hence their structures can be generated by the very short, collective displacements of specific atoms within the cell. These collective displacements through a transition state can be mediated by short wavelength (or high frequency) phonon modes for abrupt change to new phases. Using an Arhenius-type equation[10] with $\omega/2\pi \cong 10^{13}$ and $\Delta E \cong 0.1$ eV per atom, one can estimate that the phase changes or switches from semiconducting to metallic state can take place within nanoseconds. The involved energy barriers for these collective displacements of specific atoms may be lowered by the implementation of the excess charge and electrostatic interaction thereof.[10]

In the present study, the critical aspects can be emphasized as: (i) the new phases mediated specifically by excess charge from the parent t-Se and t-Te are metallic due to closing band gaps. Thus, the corresponding phase transformations result in a metal–insulator transition. (ii) Induced phases (or final states) can correspond to local minima in the Born-Oppenheimer surface only under well-defined excess charges. Therefore, these new phases are stabilized by the excess charge, but they can change back into the original semiconducting phases reversibly, if the excess charge is diminished. (iii) The phase changes are tunable, since diverse phases can be induced by changing the amount and polarity of the excess charge. (iv) Simple structural relations between the original trigonal structure of t-Se (Te) and the simple cubic or the body-centered tetragonal structure are the prime ingredient of the facile phase changes occurring with small energy raises, ΔE. (v) The amount of excess charges inducing phase changes is small and is in the range used in recent theoretical and experimental studies.[47–49] (vi) In the phases, body-centered tetragonal and the body-centered orthorhombic structures, mediated by negative charging one can identify substructures in lower dimensionality showing directional properties. (vi) When charged, surfaces of nanosheets of t-Se and t-Te, even the 2D α-tellurene monolayer undergo similar phase changes.

Clearly, t-Se and t-Te appear to be critical phase change materials offering a number of exceptional features. These features promise fundamental and potential applications. Further to the possible switch operation, a slab of t-Te may attain different phases under the perpendicular electric field, whereby electrons are transferred from one surface of the slab to other surface like a parallel plate capacitor.[44–46] At the end, a metallic cubic phase in the positively charged surface region, semiconducting trigonal phase or dielectric in the neutral middle region and metallic body centered tetragonal or orthorhombic phase at the other negatively charged surface region can be attained. In this way, a high performance nanocapacitor, a double-sided metal–semiconductor nano junction can also be generated to form a Schottky barrier or electronically composite junctions from the same parent material; its electronic properties are tuned by changing the magnitude and direction of the electric field. Also, composite materials constituted by a dielectric material sandwiched between two t-phases can offer functionalities for tunneling devices. As a final remark, 3D crystals, multilayer, bilayer and monolayer, and 1D chain structures[58–61] of Se and Te elements can reconstruct to form diverse structures with unusual properties under strain, thermal and optical excitations, excess charge and electric field.

Conflicts of interest

There are no conflicts to declare.

Acknowledgements

This work was supported by the Scientific and Technological Research Council of Turkey (TÜBİTAK) under Project No 118F097. The computational resources are provided by TÜBITAK ULAKBİM, High Performance and Grid Computing Center (TR-Grid e-Infrastructure) and the National Center for High Performance Computing of Turkey (UHeM) under Grant No. 5004132016. S. D. thanks UNAM, National Nanotechnology Center at Bilkent University for the hospitality. S. C. thanks TÜBA, Turkish Academy of Sciences The Academy of Science of Turkey for the financial Support. S. J. acknowledges support from The Academy of Science of Turkey – Outstanding Young Scientists Award Program (TÜBA-GEBIP).

References

1 M. Z. Hasan and C. L. Kane, *Rev. Mod. Phys.*, 2010, **82**, 30453067.

2 R. Keller, W. B. Holzapfel and H. Schulz, *Phys. Rev. B: Solid State*, 1977, **16**, 4404.
3 Y. Akahama, M. Kobayashi and H. Kawamura, *Phys. Rev. B: Condens. Matter Mater. Phys.*, 1993, **47**, 20–26.
4 Y. Liu, S. Hu, R. Caputo, K. Sun, Y. Li, G. Zhao and W. Ren, *RSC Adv.*, 2018, **8**, 39650–39656.
5 L. A. Agapito, N. Kioussis, W. A. Goddard and N. P. Ong, *Phys. Rev. Lett.*, 2013, **110**, 176401.
6 X. Wan, A. M. Turner, A. Vishwanath and S. Y. Savrasov, *Phys. Rev. B: Condens. Matter Mater. Phys.*, 2011, **83**, 205101.
7 M. Hirayama, R. Okugawa, S. Ishibashi, S. Murakami and T. Miyake, *Phys. Rev. Lett.*, 2015, **114**, 206401.
8 D. Lencer, M. Salinga, B. Grabowski, T. Hickel, J. Neugebauer and M. Wuttig, *Nat. Mater.*, 2008, **7**, 972–977.
9 Y. Li, K.-A. N. Duerloo, K. Wauson and E. J. Reed, *Nat. Commun.*, 2016, **7**, 10671.
10 C. X. Zhang, K. C. Santosh, Y. F. Nie, C. P. Liang, W. G. Vandenberghe, R. C. Longo, Y. P. Zheng, F. T. Kong, S. Hong, R. M. Wallace and K. Cho, *ACS Nano*, 2016, **10**, 7370–7375.
11 Y. Wang, J. Xiao, H. Zhu, Y. Li, Y. Alsaid, K. Y. Fong, Y. Zhou, S. Wang, W. Shi, Y. Wang, A. Zettl, E. J. Reed and X. Zhang, *Nature*, 2017, **550**, 487.
12 L. Z. Kou, A. J. Du, Y. D. Ma, T. Liao and C. F. Chen, *Phys. Chem. Chem. Phys.*, 2017, **19**, 22502.
13 A. Krishnamoorthy, L. Bassman, R. K. Kalia, A. Nakano, F. Shimojo and P. Vashishta, *Nanoscale*, 2018, **10**, 2742–2747.
14 Z. Zhu, X. Cai, S. Yi, J. Chen, Y. Dai, C. Niu, Z. Guo, M. Xie, F. Liu, J.-H. Cho, Y. Jia and Z. Zhang, *Phys. Rev. Lett.*, 2017, **119**, 106101.
15 C. Wang, X. Zhou, J. Qiao, L. Zhou, X. Kong, Y. Pan, Z. Cheng, Y. Chai and W. Ji, *Nanoscale*, 2018, **10**, 22263–22269.
16 A. K. Geim and I. V. Grigoreva, *Nature*, 2013, **499**, 419–425.
17 C. Zhang, H. Huang, X. Ni, Y. Zhou, L. Kang, W. Jiang, H. Chen, J. Zhong and F. Liu, *Nanoscale*, 2018, **10**, 16759–16764.
18 P. Skadron and V. A. Johnson, *J. Appl. Phys.*, 1966, **37**, 1912.
19 Y. Liu, W. Wu and W. A. Goddard, *J. Am. Chem. Soc.*, 2018, **140**, 550–553.
20 J. P. Perdew, K. Burke and M. Ernzerhof, *Phys. Rev. Lett.*, 1996, **77**, 3865–3868.
21 A. V. Krukau, O. A. Vydrov, A. F. Izmaylov and G. E. Scuseria, *J. Chem. Phys.*, 2006, **125**, 224106.
22 G. Kresse and J. Hafner, *Phys. Rev. B: Condens. Matter Mater. Phys.*, 1993, **47**, 558–561.
23 G. Kresse and J. Hafner, *Phys. Rev. B: Condens. Matter Mater. Phys.*, 1994, **49**, 14251–14269.
24 G. Kresse and J. Furthmüller, *Comput. Mater. Sci.*, 1996, **6**, 15–50.
25 G. Kresse and J. Furthmüller, *Phys. Rev. B: Condens. Matter Mater. Phys.*, 1996, **54**, 11169–11186.
26 J. M. Soler, E. Artacho, J. D. Gale, A. García, J. Junquera, P. Ordejón and D. Sánchez-Portal, *J. Phys.: Condens. Matter*, 2002, **14**, 2745–2779.
27 P. E. Blöchl, *Phys. Rev. B: Condens. Matter Mater. Phys.*, 1994, **50**, 17953–17979.
28 H. J. Monkhorst and J. D. Pack, *Phys. Rev. B: Solid State*, 1976, **13**, 5188–5192.
29 T. Bucko, S. Lebegue, J. Hafner and J. G. Angyan, *J. Chem. Theory Comput.*, 2013, **9**, 4293–4299.
30 T. Bucko, S. Lebegue, J. G. Angyan and J. Hafner, *J. Chem. Phys.*, 2014, **141**, 034114.
31 M. Topsakal, H. H. Gürel and S. Ciraci, *J. Phys. Chem. C*, 2013, **117**, 5943–5952.
32 N. Troullier and J. L. Martins, *Phys. Rev. B: Condens. Matter Mater. Phys.*, 1991, **43**, 1993.
33 M. Dion, H. Rydberg, E. Schröder, D. C. Langreth and B. I. Lundqvist, *Phys. Rev. Lett.*, 2004, **92**, 246401.
34 G. Román-Pérez and J. M. Soler, *Phys. Rev. Lett.*, 2009, **103**, 096102.
35 D. Alfè, *Comput. Phys. Commun.*, 2009, **180**, 2622.
36 S. Tutihasi and I. Chen, *Phys. Rev.*, 1967, **158**, 623.
37 V. B. Anzin, M. I. Eremets, Y. V. Hosichkin, A. I. Nadezhdinskii and A. M. Shirokov, *Phys. Status Solidi A*, 1977, **42**, 385–390.
38 D. Legut, M. Friák and M. Šob, *Phys. Rev. Lett.*, 2007, **99**, 016902.
39 W. A. Harrison, *Electronic structure and the properties of solids: The pyhsics of the chemical bond*, W.H. Freeman and Company, San Francisco, 1980.
40 F. Carbone, P. Baum, P. Rudolf and A. H. Zewail, *Phys. Rev. Lett.*, 2008, **100**, 035501–035504.
41 M. Topsakal and S. Ciraci, *Appl. Phys. Lett.*, 2011, **98**, 131908.
42 Z. Wei, D. Wang, S. Kim, S.-Y. Kim, Y. Hu, M. K. Yakes, A. R. Laracuente, Z. Dai, S. R. Marder, C. Berger, W. P. King, W. A. de Heer, P. E. Sheehan and E. Riedo, *Science*, 2010, **328**, 1373–1376.
43 Ö. Ekiz, M. Ürel, H. Güner, A. K. Mizrak and A. Dâna, *ACS Nano*, 2011, **5**, 2475.
44 V. O. Özçelik and S. Ciraci, Nanoscale Dielectric Capacitors Composed of Graphene and Boron Nitride Layers, *J. Phys. Chem. C*, 2013, **117**, 15327–15334.
45 V. O. Özçelik and S. Ciraci, *Phys. Rev. B: Condens. Matter Mater. Phys.*, 2015, **91**, 195445.
46 T. Teshome and A. Datta, *ACS Appl. Mater. Interfaces*, 2017, **9**, 34213–34220.
47 N. D. Drummond, V. Zólyomi and V. I. Fal'ko, *Phys. Rev. B: Condens. Matter Mater. Phys.*, 2012, **85**, 075423.
48 F. Peymanirad, M. Neek-Amal, J. Beheshtian and F. M. Peeters, *Phys. Rev. B: Condens. Matter Mater. Phys.*, 2015, **92**, 155113.
49 N. Luo, C. Si and W. Duan, *Phys. Rev. B*, 2017, **95**, 205432.
50 F. Bruneval, C. Varvenne, J.-P. Crocombette and E. Clouet, *Phys. Rev. B: Condens. Matter Mater. Phys.*, 2015, **91**, 024107.
51 H. Hu, M. Liu, Z. F. Wang, J. Zhu, D. Wu, H. Ding, Z. Liu and F. Liu, *Phys. Rev. Lett.*, 2012, **109**, 055501.

52 L. Xian, A. Pérez Paz, E. Bianco, P. M. Ajayan and A. Rubio, *2D Mater.*, 2017, **4**, 041003.
53 Z. Zhang, S. N. Shirodkar, Y. Yang and B. I. Jakobsen, *Angew. Chem.*, 2017, **129**, 15623–15628.
54 D. Liu and D. Tomanek, *Nano Lett.*, 2019, **19**, 1359–1365.
55 A. Pachoud, M. Jaiswal, P. K. Ang, K. P. Loh and B. Oezyilmaz, *EPL*, 2010, **92**, 27001.
56 N. Shukla, A. V. Thathachary, A. Agrawal, H. Paik, A. Aziz, D. G. Schlom, S. K. Gupta, R. E. Herbert and S. Datta, *Nat. Commun.*, 2015, **6**, 7812.
57 J.-P. Gaspard, *C. R. Phys.*, 2016, **17**, 389–405.
58 E. Andharia, T. P. Kaloni, G. J. Salamo, S.-Q. Yu, H. O. H. Churchill and S. Barraza-Lopez, *Phys. Rev. B*, 2018, **98**, 035420.
59 D. Liu, X. Lin and D. Tománek, *Nano Lett.*, 2018, **18**, 4908–4913.
60 Y. Pan, S. Gao, L. Yang and J. Lu, *Phys. Rev. B*, 2018, **98**, 085135.
61 L. Qi, J. Han, W. Gao and Q. Jiang, *Nanoscale*, 2019, **11**, 4053.